# Supporting Information

## Yukl et al. 10.1073/pnas.1215011110

### SI Methods

**Protein Expression and Purification.** Recombinant diheme enzyme MauG (1) was purified from *Paracoccus denitrificans* as described previously. Pre-methylamine dehydrogenase (preMADH) (2) was expressed in *Rhodobacter sphaeroides* and purified as described previously (3).

**UV-Visible Absorbance Spectroscopy.** For single-turnover reactions, preMADH and MauG were combined at a final concentration of 10 and 1.0 μM, respectively, in 10 mM potassium phosphate buffer at pH 7.5. $H_2O_2$ from a concentrated stock solution was added to a final concentration of 10 μM, and the absorbance spectrum recorded on a Cary 50 UV-visible spectrophotometer (Varian). Hydroxyurea was then added at a concentration of 2.0 mM and the spectrum recorded. The pre–steady-state reaction contained 30 μM preMADH, 3.0 μM MauG, and 1.0 mM $H_2O_2$. After an ~30-s reaction time, hydroxyurea was added to 3.0 mM and the spectrum recorded.

**Electron Paramagnetic Resonance Spectroscopy.** The high-frequency and -field electron paramagnetic resonance (HFEPR) sample was prepared in a two-step sequential mixing experiment. First, MauG (135 μL, 1.43 mM) was added to preMADH (170 μL, 1.17 mM) in a HFEPR sample cup, which created an enzyme–substrate complex (0.78 mM, 1:1 mixing). In the second step, $H_2O_2$ (final concentration, 1.22 mM) was added from a freshly prepared stock solution (25 mM), and the mixture was frozen by liquid nitrogen. The freezing process took 10–12 s.

The HFEPR spectra were recorded at the Electron Magnetic Resonance Facility at the National High Magnetic Field Laboratory, Tallahassee, FL (4). The HFEPR spectrometer has been described elsewhere (5). The spectra were recorded in the presence of a standard described in Stoll et al. (6) to ensure proper magnetic field calibration. HFEPR simulations were performed using the EPR simulation program DOUBLET (7).

The EPR sample for continuous-wave X-band EPR quantitative analysis was made in a reaction vial to a final protein concentration of 150 μM for both MauG and preMADH with addition of 1 equivalent of $H_2O_2$. The sample was transferred into a standard quartz EPR tube and frozen by liquid nitrogen. The process of mixing and freezing was complete within 10–12 s. The X-band spectrum was recorded at liquid helium temperatures on a Bruker ER200D spectrometer at 100-kHz modulation frequency using a 4116DM resonator. Sample temperature was maintained by an ITC503S controller, an ESR910 cryostat, and a LLT650/13 liquid helium transfer tube (Oxford Instruments). The sample was analyzed at both perpendicular and parallel modes. Spin concentration was determined by double integration of the sample spectrum obtained under nonsaturating conditions and comparing the resulting intensity to the $g = 2$ EPR signal ($S = 1/2$) of a copper standard (1 mM $CuSO_4$, 10 mM EDTA) recorded under the same instrument conditions.

**Mass Spectrometry.** Reaction mixtures contained 25–55 μL of 20 μM preMADH, 40 μM MauG, and 0–120 μM $H_2O_2$ in 10 mM potassium phosphate buffer (pH 7.5). $H_2O_2$ was added to MauG followed by addition of preMADH. Samples were incubated for 1 h before injection onto a C4 column (Phenomenex) connected to a HPLC system (Waters). A gradient of 5–40% acetonitrile was applied, and the absorbance at 280 nm was monitored. Fractions of 30 s were collected, speed vacuumed to dryness, and reconstituted in 50% acetonitrile, 0.1% formic acid before introduction into the mass spectrometer.

Data were acquired on a QSTAR XL (AB Sciex) quadrupole TOF mass spectrometer with the IonSpray electrospray source. Samples were manually injected into a 10-μL sample loop plumbed into the divert/inject valve of the instrument. Samples were infused at a flow rate of 10 μL/min with 50:50 acetonitrile: water, 0.1% formic acid. The IonSpray voltage was 4700 V. The TOF region acceleration voltage was 4 kV, and the injection pulse repetition rate was 4.9 kHz. The monoisotopic peaks of human renin substrate tetradecapeptide from Sigma-Aldrich were used for external calibration ([M + 3H]$^{3+}$ at 586.9830 and [M + 2H]$^{2+}$ at 879.9705). TOF MS spectra were acquired from 700–2200 *m/z* for ~5 min with a 1-s accumulation time. The acquisition software was Analyst QS v1.0 (AB Sciex). The Bayesian protein reconstruct tool in BioAnalyst extensions v1.1 (AB Sciex) was used for multiple charge-state data deconvolution of the intact proteins.

**Crystallization, X-Ray Data Collection, and Structure Determination.** A 2:1 MauG/preMADH ratio mix was used in crystallization. The WT MauG and W199F MauG complexes with preMADH were crystallized as previously reported using hanging-drop vapor diffusion in VDX plates (Hampton Research) (8, 9). Single crystals suitable for X-ray data collection were obtained from drops assembled with 1 μL protein solution layered with 3 μL reservoir solution over a 22–26% wt/vol PEG 8000, 0.1 M sodium acetate, 0.1 M Mes (pH 6.4) reservoir. WT MauG–preMADH crystals were harvested every 10 d for 50 d, and once at 130 d following crystallization tray setup, and were cryoprotected as described previously through the inclusion of 10% PEG 400 (8). The W199F MauG–preMADH crystal was harvested after 60 d.
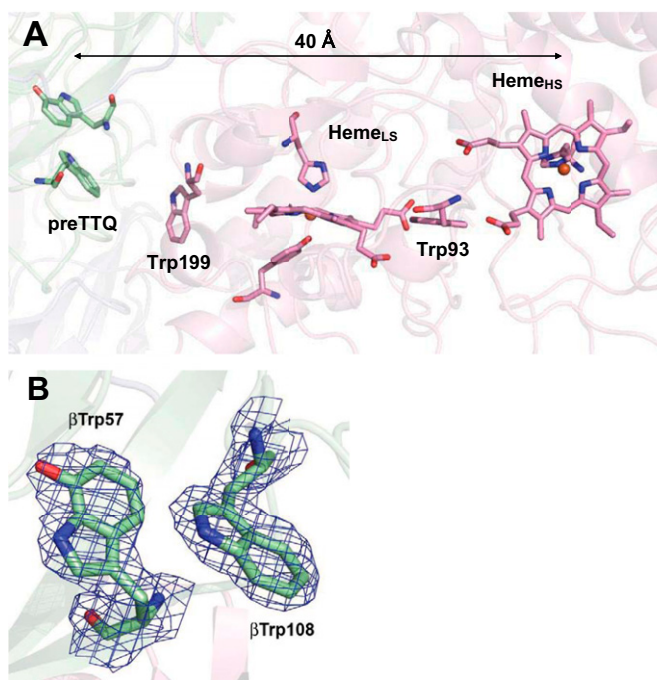
X-ray diffraction data were collected at GM/CA-CAT beamlines 23-ID-D and 23-ID-B of the Advanced Photon Source, Argonne National Laboratory. Data were collected at 100 K using a beam size matching the dimensions of the largest crystal face. The diffraction data are in the space group P1 with one complex (two MauGs bound to one preMADH) in the asymmetric unit. The data were processed with HKL2000 (10).

Initial refinement was carried out using REFMAC (11) in the CCP4 program suite (12) using the model of WT MauG–preMADH (3L4M), and model-building was carried out in COOT (13, 14). MADH residues βTrpOH-57 [designated amino acid type 0AF in the Protein Data Bank (PDB)] and βTrp-108 were built as pre-tryptophan tryptophylquinone (preTTQ) with no link between residues; as a cross-linked species with a link at 1.47 Å between residues; as mature TTQ with a link between residues and a second oxygen atom inserted into βTrp-57 (designated amino acid type TRQ in the PDB); or a combination of the above with occupancies adjusted to result in B-factors comparable to each other and surrounding residues (Table S1). X-ray diffraction data for the 20- and 30-d aged crystals were clearly a mix of preTTQ and cross-linked preTTQ, with the final refined models containing 60:40% and 40:60% preTTQ and cross-linked preTTQ, respectively. Although the 50-d-aged crystal clearly had significant electron density for the second oxygen, it was decided to include only a single predominant model in the final refinement, because B-factor matching was based on a single atom (all of the other atom positions of cross-linked preTTQ and TTQ are coincident). Restrained refinement with TLS was carried out using no distance restraints between the heme iron centers and

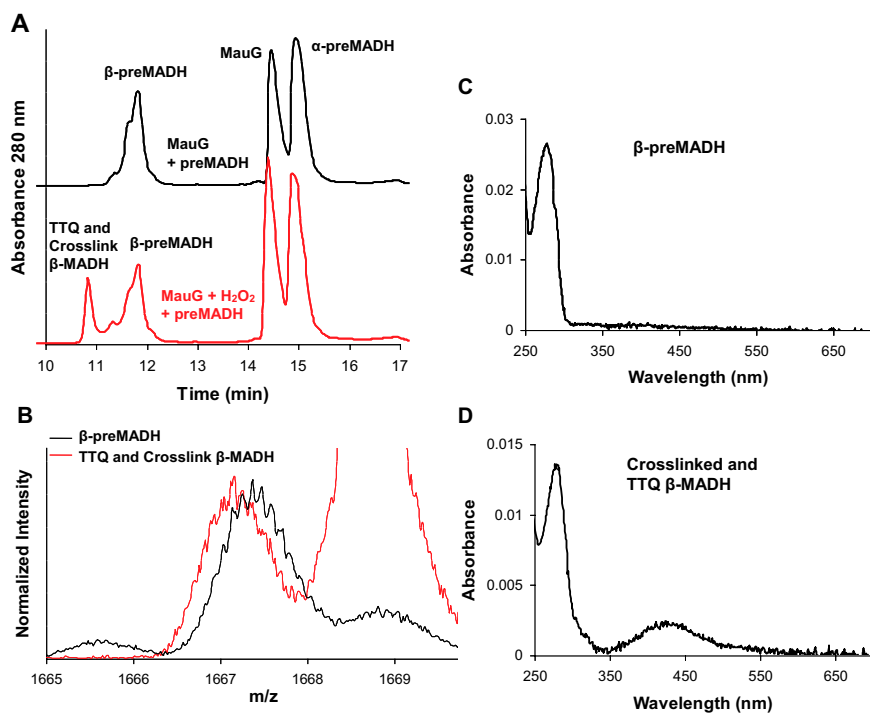their ligands. Refinement was assessed as complete when the Fo–Fc electron density contained only noise. Calculated electron density maps used in Fig. 2A and Fig. S1B were generated in PHENIX (15).

1. Wang YT, et al. (2003) MauG, a novel diheme protein required for tryptophan tryptophylquinone biogenesis. *Biochemistry* 42(24):7318–7325.
2. Pearson AR, et al. (2004) Further insights into quinone cofactor biogenesis: Probing the role of MauG in methylamine dehydrogenase tryptophan tryptophylquinone formation. *Biochemistry* 43(18):5494–5502.
3. Graichen ME, et al. (1999) Heterologous expression of correctly assembled methylamine dehydrogenase in *Rhodobacter sphaeroides. J Bacteriol* 181(14): 4216–4222.
4. Hassan AK, et al. (2000) Ultrawide band multifrequency high-field EMR technique: A methodology for increasing spectroscopic information. *J Magn Reson* 142(2):300–312.
5. Chen Y, et al. (2012) Role of calcium in metalloenzymes: Effects of calcium removal on the axial ligation geometry and magnetic properties of the catalytic diheme center in MauG. *Biochemistry* 51(8):1586–1597.
6. Stoll S, Ozarowski A, Britt RD, Angerhofer A (2010) Atomic hydrogen as high-precision field standard for high-field EPR. *J Magn Reson* 207(1):158–163.
7. Ozarowski A, Lee HM, Balch AL (2003) Crystal environments probed by EPR spectroscopy. Variations in the EPR spectra of Co(II)(octaethylporphyrin) doped in crystalline diamagnetic hosts and a reassessment of the electronic structure of four-coordinate cobalt(II). *J Am Chem Soc* 125(41):12606–12614.
8. Jensen LMR, Sanishvili R, Davidson VL, Wilmot CM (2010) *In crystallo* posttranslational modification within a MauG/pre-methylamine dehydrogenase complex. *Science* 327 (5971):1392–1394.
9. Tarboush NA, et al. (2011) Mutagenesis of tryptophan199 suggests that hopping is required for MauG-dependent tryptophan tryptophylquinone biosynthesis. *Proc Natl Acad Sci USA* 108(41):16956–16961.
10. Otwinowski Z, Minor W (1997) Processing of X-ray diffraction data collected in oscillation mode. *Macromol Cryst Pt A* 276:307–326.
11. Murshudov GN, Vagin AA, Dodson EJ (1997) Refinement of macromolecular structures by the maximum-likelihood method. *Acta Crystallogr D Biol Crystallogr* 53(Pt 3):240–255.
12. Collaborative Computational Project, Number 4 (1994) The CCP4 suite: Programs for protein crystallography. *Acta Crystallogr D Biol Crystallogr* 50(Pt 5):760–763.
13. Emsley P, Cowtan K (2004) COOT: Model-building tools for molecular graphics. *Acta Crystallogr D Biol Crystallogr* 60(Pt 12 1):2126–2132.
14. Emsley P, Lohkamp B, Scott WG, Cowtan K (2010) Features and development of Coot. *Acta Crystallogr D Biol Crystallogr* 66(Pt 4):486–501.
15. Adams PD, et al. (2010) PHENIX: A comprehensive Python-based system for macromolecular structure solution. *Acta Crystallogr D Biol Crystallogr* 66(Pt 2): 213–221.
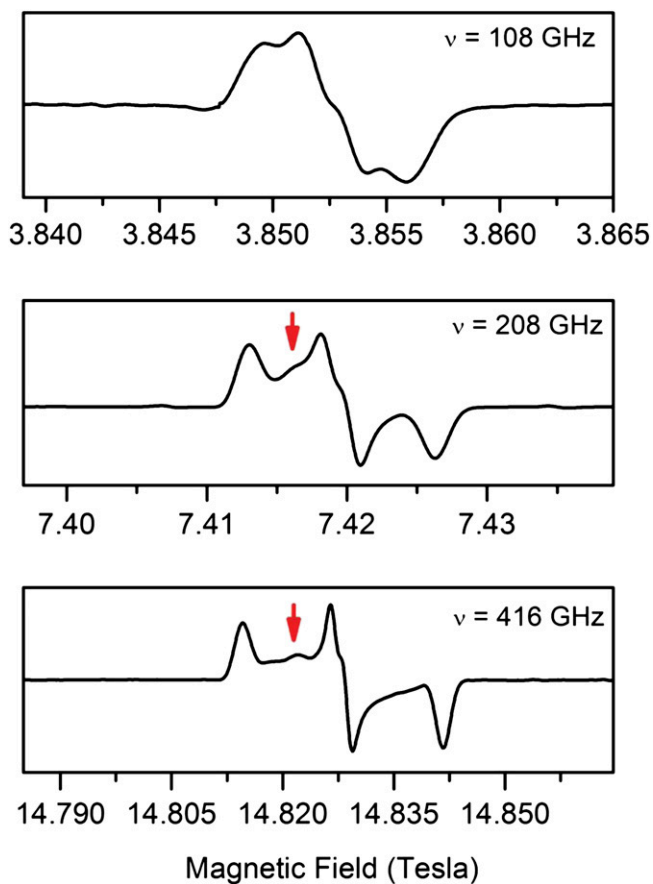
**Fig. S1.** (A) MauG–preMADH structure (PDB ID code 3L4M) showing the electron transfer pathway from preTTQ to the MauG hemes (1). (B) Calculated electron density from a W199F MauG–preMADH crystal harvested after 60 d following crystallization setup, using the refined WT MauG–preMADH 10 d model to calculate phases. Structure drawn as secondary structure cartoon; MauG, pink; MADH β, green; MADH α, blue. MauG hemes and residues are drawn in stick colored according to element. 2Fo–Fc electron density (blue) contoured at 1.0σ. The figure was produced using PyMOL (www.pymol.org).

1. Jensen LMR, Sanishvili R, Davidson VL, Wilmot CM (2010) *In crystallo* posttranslational modification within a MauG/pre-methylamine dehydrogenase complex. *Science* 327(5971): 1392–1394.

**Fig. S2.** (*A*) Reverse-phase chromatographic separation of MauG and MADH subunits from reaction mixtures containing MauG, preMADH, and $H_2O_2$ in a 2:1:0 (black) and 2:1:2 (red) ratio. (*B*) Mass spectrum of the two peaks labeled β-preMADH (black) and TTQ and cross-link β-MADH (red) of a reaction mixture containing MauG, preMADH, and $H_2O_2$ in a 2:1:2 ratio. UV-visible absorbance of peak C4 column fractions labeled (*C*) β-preMADH and (*D*) TTQ and cross-link β-MADH.



**Fig. S3.** Multifrequency EPR spectra (108–416 GHz) of the preMADH radicals recorded at 10 K. Arrows indicate the resolved new $g_z$ component for a second radical species as the magnetic field applied to the sample is increased.

**Fig. S4.** Simulation (red trace) of an HFEPR spectrum (10 K, 406.4 GHz) including only one distinct radical with EPR parameters of $g_x = 2.00216$, $g_y = 2.00398$, $g_z = 2.00581$, and $A_{yy} = 15$ G is unable to account for all of the resonances, indicating a second distinct radical must be present. The field calibration standard described in *SI Methods* is present as two sharp lines on either side of the radical spectrum.



**Fig. S5.** (*A*) 77-K HFEPR spectrum of the preMADH-based diradical intermediate at 406.4 GHz, including the field standard. Spectral simulation (*E*) shows the presence of two free radical species (*B* and *C*), the H-standard and a minor manganese (Mn) signal (*D*). The final simulated spectrum with $0.85(B) + 0.15(C) + (D)$ is shown in trace *E*. The well-resolved $A_{yy}$ couplings at a higher temperature indicate the EPR signals are derived from two distinct free radicals rather than an exchange-coupled radical pair or a triplet state. Note that the difference in ratio between the two radical species at very high-field EPR may be due to differences in power saturation properties or differential stability of the two radical species.

**Table S1. X-ray crystallography data collection and refinement statistics**

| Data collection | WT MauG–preMADH aged 10 d | WT MauG–preMADH aged 20 d | WT MauG–preMADH aged 30 d |
|---|---|---|---|
| Detector type | MAR*mosaic* 4 × 4 tiled CCD | MAR*mosaic* 4 × 4 tiled CCD | MAR*mosaic* 4 × 4 tiled CCD |
| Source | APS, sector 23 | APS, sector 23 | APS, sector 23 |
| Space group | P1 | P1 | P1 |
| Unit cell lengths, Å | 56.02 × 84.93 × 108.49 | 56.00 × 84.92 × 108.41 | 55.77 × 84.49 × 108.25 |
| Unit cell angles, ° | 110.93, 91.61, 104.90 | 111.02, 91.57, 105.00 | 110.64, 91.66, 104.88 |
| Wavelength, Å | 1.03320 | 1.03320 | 1.03320 |
| Resolution, Å | 50.00–2.14 (2.18–2.14) | 50.00–1.94 (1.97–1.94) | 50.00–2.09 (2.13–2.09) |
| Measured reflections | 233,482 | 503,083 | 399,901 |
| Unique reflections | 98,967 | 132,248 | 105,482 |
| Completeness, % | 97.4 (95.7) | 97.2 (88.5) | 97.3 (89.6) |
| $R_{merge}$, %* | 9.6 (40.0) | 8.6 (44.3) | 7.9 (46.6) |
| I/σI | 9.6 (2.1) | 21.1 (2.4) | 16.7 (2.4) |
| Multiplicity | 2.4 (2.2) | 3.9 (3.5) | 3.9 (3.5) |
| Refinement[†] | | | |
|   Resolution, Å | 43.46–2.14 (2.20–2.14) | 44.49–1.94 (1.99–1.94) | 44.49–2.09 (2.14–2.09) |
|   No. reflections; working/test | 88,625/4,717 | 119,177/6,283 | 95,313/5,057 |
|   $R_{work}$, %[‡] | 16.3 | 15.2 | 15.7 |
|   $R_{free}$, %[§] | 22.7 | 20.4 | 21.4 |
|   Protein atoms | 13,497 | 13,525 | 13,476 |
|   Ligand atoms | 208 | 209 | 208 |
|   Solvent sites | 1,049 | 1,318 | 841 |
| Ramachandran statistics[¶] | | | |
|   Allowed, % | 99.0 | 99.1 | 98.8 |
|   Outliers, % | 1.0 | 0.9 | 1.2 |
| Rmsd | | | |
|   Bond lengths, Å | 0.020 | 0.022 | 0.022 |
|   Bond angles, ° | 2.008 | 2.111 | 2.064 |
|   Average B-factor, Å$^2$ | 36.89 | 33.23 | 39.02 |
|   Estimated standard uncertainty, Å/$R_{work}$/$R_{free}$[‖] | 0.254/0.203 | 0.153/0.144 | 0.211/0.179 |
|   PDB ID code | 4FA4 | 4FA5 | 4FA9 |
| Modeling** | | | |
|   PreTTQ, % | 100 | 60 | 40 |
|   Cross-linked, % | 0 | 40 | 60 |
|   TTQ, % | 0 | 0 | 0 |

Values in parentheses are for the highest-resolution shell. APS, Advanced Photon Source.

*$R_{merge} = \Sigma_i\ I_{hkl,i} - \langle I_{hkl}\rangle|/\Sigma_{hkl}\ \Sigma_i\ I_{hkl,i}$, where I is the observed intensity and ‹Ihkl› is the average intensity of multiple measurements.

[†]The cell constants for all WT preMADH structures were isomorphous with previously reported WT MauG-preMADH, and therefore set to those of PDB ID code 3L4M.

[‡]$R_{work} = \Sigma||F_o|-|F_c||/\Sigma|F_o|$, where $|F_o|$ is the observed structure factor amplitude, and $|F_c|$ is the calculated structure factor amplitude.

[§]$R_{free}$ is the R factor based on 5% of the data excluded from refinement. The data were equivalent to the free R set used in the determination of WT MauG–preMADH (PDB ID code 3L4M).

[¶]Based on values attained from refinement validation options in COOT.

[‖]Estimated standard uncertainties generated for $R_{work}$ and $R_{free}$ in Refmac5.5 in the CCP4i (1) suite.

**PreTTQ-derived species that were in the final refined model.

1. Collaborative Computational Project, Number 4 (1994) The CCP4 suite: Programs for protein crystallography. *Acta Crystallogr D Biol Crystallogr* 50(Pt 5):760–763.

**Table S2. X-ray crystallography data collection and refinement statistics**

| Data collection | WT MauG–preMADH aged 40 d | WT MauG–preMADH aged 50 d | WT MauG–preMADH aged 130 d |
|---|---|---|---|
| Detector type | MARmosaic 4 × 4 tiled CCD | MARmosaic 4 × 4 tiled CCD | MARmosaic 4 × 4 tiled CCD |
| Source | APS, sector 23 | APS, sector 23 | APS, sector 23 |
| Space group | P1 | P1 | P1 |
| Unit cell lengths, Å | 56.04 × 84.91 × 108.36 | 56.12 × 85.10 × 108.19 | 55.81 × 84.92 × 108.22 |
| Unit cell angles, ° | 110.99, 91.60, 104.76 | 111.05, 91.83, 104.50 | 110.99, 91.76, 104.68 |
| Wavelength, Å | 1.03313 | 1.03313 | 1.03320 |
| Resolution, Å | 50.00–2.08 (2.12–2.08) | 50.00–2.08 (2.12–2.08) | 50.00–2.18 (2.22–2.18) |
| Measured reflections | 434,009 | 436,246 | 181,981 |
| Unique reflections | 106,696 | 107,370 | 92,667 |
| Completeness, % | 96.9 (90.5) | 96.9 (89.3) | 92.8 (69.3) |
| $R_{merge}$, %* | 9.6 (57.1) | 6.7 (57.8) | 7.1 (35.3) |
| I/σI | 14.4 (2.2) | 18.7 (2.1) | 11.6 (2.0) |
| Multiplicity | 4.2 (3.5) | 4.2 (3.6) | 2.1 (2.0) |
| Refinement[†] | | | |
|   Resolution, Å | 44.49–2.08 (2.13–2.08) | 44.49–2.08 (2.13–2.08) | 37.17–2.18 (2.24–2.18) |
|   No. reflections; working/test | 96,231/5,095 | 96,263/5,105 | 80,674/4,239 |
|   $R_{work}$,%[‡] | 17.0 | 16.3 | 15.7 |
|   $R_{free}$, %[§] | 23.4 | 22.4 | 22.7 |
|   Protein atoms | 13,409 | 13,403 | 13,414 |
|   Ligand atoms | 218 | 214 | 196 |
|   Solvent sites | 919 | 763 | 996 |
| Ramachandran statistics[¶] | | | |
|   Allowed, % | 99.10 | 99.09 | 98.91 |
|   Outliers, % | 0.90 | 0.91 | 1.09 |
| Rmsd | | | |
|   Bond lengths, Å | 0.022 | 0.022 | 0.019 |
|   Bond angles, ° | 2.061 | 2.088 | 1.932 |
|   Average B-factor, Å² | 41.88 | 45.09 | 37.75 |
|   Estimated standard uncertainty, Å/$R_{work}$/$R_{free}$[‖] | 0.224/0.195 | 0.213/0.186 | 0.290/0.219 |
|   PDB ID code | 4FAN | 4FAV | 4FA1 |
| Modeling** | | | |
|   PreTTQ, % | 0 | 0 | 0 |
|   Cross-linked, % | 100 | 100 | 0 |
|   TTQ, % | 0 | 0 | 100 |

Values in parentheses are for the highest-resolution shell. APS, Advanced Photon Source.

*$R_{merge} = \Sigma_i\ I_{hkl,i} - \langle I_{hkl}\rangle/\Sigma_{hkl}\ \Sigma_i\ I_{hkl,i}$, where I is the observed intensity and ‹hkl› is the average intensity of multiple measurements.

[†]The cell constants for all WT preMADH structures were isomorphous with previously reported WT MauG-preMADH, and therefore set to those of PDB ID code 3L4M.

[‡]$R_{work} = \Sigma||F_o|-|F_c||/\Sigma|F_o|$, where $|F_o|$ is the observed structure factor amplitude, and $|F_c|$ is the calculated structure factor amplitude.

[§]$R_{free}$ is the R factor based on 5% of the data excluded from refinement. The data were equivalent to the free R set used in the determination of WT MauG–preMADH (PDB ID code 3L4M).

[¶]Based on values attained from refinement validation options in COOT.

[‖]Estimated standard uncertainties generated for $R_{work}$ and $R_{free}$ in Refmac5.5 in the CCP4i (1) suite.

**PreTTQ-derived species that were in the final refined model.

1. Collaborative Computational Project, Number 4 (1994) The CCP4 suite: Programs for protein crystallography. *Acta Crystallogr D Biol Crystallogr* 50(Pt 5):760–763.
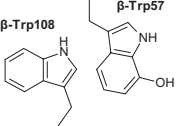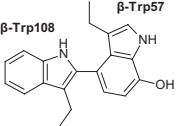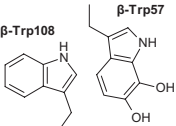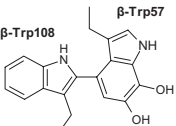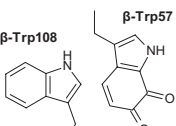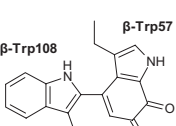
**Table S3.   X-ray crystallography data collection statistics**

| Data collection | W199F MauG–preMADH aged 60 d |
|---|---|
| Detector type | MAR*mosaic* 4 × 4 tiled CCD |
| Source | APS, sector 23 |
| Space group | *P*1 |
| Unit cell lengths, Å | 55.69 × 84.00 × 108.07 |
| Unit cell angles, ° | 110.35, 91.65, 105.21 |
| Wavelength, Å | 1.03320 |
| Resolution, Å | 50.00–2.24 (2.28–2.24) |
| Measured reflections | 179,550 |
| Unique reflections | 83,019 |
| Completeness, % | 97.7 (96.7) |
| $R_{merge}$, %* | 7.8 (39.9) |
| I/σI | 11.0 (2.1) |
| Multiplicity | 2.2 (2.0) |

Values in parentheses are for the highest-resolution shell. APS, Advanced Photon Source.

*$R_{merge} = \Sigma_i \ I_{hkl,i} - \langle I_{hkl} \rangle / \Sigma_{hkl} \ \Sigma_i \ I_{hkl,i}$, where I is the observed intensity and $\langle I_{hkl} \rangle$ is the average intensity of multiple measurements.

**Table S4. Calculated and observed masses for potential intermediates in TTQ biogenesis**

| Species | Calculated mass | Observed mass ± SD |
|---|---|---|
|  | 14,997.5 | 14,997.54 ± 0.02 |
|  | 14,995.5 | 14,995.60 ± 0.05 |
|  | 15,013.5 | Not observed |
|  | 15,011.5 | Not observed |
|  | 15,011.5 | Not observed |
|  | 15,009.5 | 15,009.73 ± 0.20 |

**Table S5.** *g* tensors obtained by HFEPR from representative enzymes and models

| Radical | $g_x$ | $g_y$ | $g_z$ | $\Delta g$ $(g_x–g_z)$ | Source |
|---|---|---|---|---|---|
| **Trp** | | | | | |
| preMADH Trp108 | 2.00486 | 2.00402 | 2.00216 | 0.00270 | This work |
| preMADH Trp57-OH | 2.00581 | 2.00398 | 2.00216 | 0.00365 | This work |
| Versatile peroxidase Trp | 2.00352 | 2.00255 | 2.00220 | 0.00132 | 1 |
| *Bulkholderia pseudomallei* KatG Trp | 2.0036(3) | 2.0027(6) | 2.0022(0) | 0.0014 | 2 |
| Ribonucleotide reductase W111 Trp | 2.0033 | 2.0024 | 2.0021 | 0.0012 | 3 |
| Re-Azurin Trp108 | 2.00346 | 2.00264 | 2.00216 | 0.00130 | 4 |
| Re-Azurin Trp48 | 2.00361 | 2.00270 | 2.00215 | 0.00146 | 4 |
| Cytochrome *c* peroxidase Trp | 2.0033 | 2.0024 | 2.0021 | 0.0012 | 5 |
| Lignin peroxidase Trp | 2.0035(5) | 2.0027(5) | 2.0022(1) | 0.0013(5) | 6 |
| **Tyr** | | | | | |
| *Escherichia coli* ribonucleotide reductase Tyr | 2.00912 | 2.00457 | 2.00225 | 0.00687 | 7 |
| *Salmonella typhimurium* ribonucleotide reductase Tyr | 2.0089 | 2.0043 | 2.0021 | 0.0068 | 8 |
| *Mycobacterium tuberculosis* ribonucleotide reductase Tyr | 2.00920 | 2.00460 | 2.00220 | 0.0070 | 9 |
| Ribonucleotide reductase Tyr from virus | 2.0080 | 2.0043 | 2.0021 | 0.0059 | 10 |
| PSII Tyr-D | 2.00740 | 2.00425 | 2.00205 | 0.00529 | 11 |
| PSII (Y190F) Tyr-Z | 2.00750 | 2.00422 | 2.00225 | 0.00525 | 11 |
| KatG Tyr | 2.0064 | 2.0040 | 2.0020 | 0.0044 | 12 |
| Prostaglandin $H_2$ synthase-1 Tyr | 2.0078 | 2.0043 | 2.0021 | 0.0057 | 13 |
| Cytochrome *c* oxidase Tyr (pH 8) | 2.0059 | 2.0051 | 2.0017 | 0.0042 | 14 |
| Cytochrome *c* oxidase Tyr (pH 6) | 2.0072 | 2.0041 | 2.0023 | 0.0049 | 14 |
| Bovine liver catalase Tyr | 2.00777 | 2.0046 | 2.00232 | 0.00545 | 15 |
| P450$_{cam}$ Tyr96 | 2.00780 | 2.00440 | 2.00219 | 0.0056 | 16 |
| Turnip isoperoxidase 7 Tyr | 2.0066 | 2.0043 | 2.0020 | 0.0046 | 17 |
| γ-Irradiated single crystal of Tyr·HCl | 2.0067 | 2.0045 | 2.0023 | 0.0044 | 18 |

Value in parentheses are standard errors.

1. Pogni R, et al. (2006) A tryptophan neutral radical in the oxidized state of versatile peroxidase from *Pleurotus eryngii*: A combined multifrequency EPR and density functional theory study. *J Biol Chem* 281(14):9517–9526.
2. Colin J, Wiseman B, Switala J, Loewen PC, Ivancich A (2009) Distinct role of specific tryptophans in facilitating electron transfer or as [Fe(IV)=O Trp(*)] intermediates in the peroxidase reaction of *Bulkholderia pseudomallei* catalase-peroxidase: A multifrequency EPR spectroscopy investigation. *J Am Chem Soc* 131(24):8557–8563.
3. Bleifuss G, et al. (2011) Tryptophan and tyrosine radicals in ribonucleotide reductase: A comparative high-field EPR study at 94 GHz. *Biochemistry* 40(50):15362–15368.
4. Stoll S, et al. (2011) Hydrogen bonding of tryptophan radicals revealed by EPR at 700 GHz. *J Am Chem Soc* 133(45):18098–18101.
5. Ivancich A, Dorlet P, Goodin DB, Un S (2001) Multifrequency high-field EPR study of the tryptophanyl and tyrosyl radical intermediates in wild-type and the W191G mutant of cytochrome *c* peroxidase. *J Am Chem Soc* 123(21):5050–5058.
6. Smith AT, Doyle WA, Dorlet P, Ivancich A (2009) Spectroscopic evidence for an engineered, catalytically active Trp radical that creates the unique reactivity of lignin peroxidase. *Proc Natl Acad Sci USA* 106(38):16084–16089.
7. Gerfen GJ, et al. (1993) High-frequency (139.5 GHz) EPR spectroscopy of the tyrosyl radical in *Escherichia coli* ribonucleotide reductase. *J Am Chem Soc* 115:6420–6421.
8. Allard P, et al. (1996) Characterization of a new tyrosyl free radical in *Salmonella typhimurium* ribonucleotide reductase with EPR at 9.45 and 245 GHz. *J Am Chem Soc* 118:895–896.
9. Liu AM, Barra AL, Rubin H, Lu GZ, Gräslund A (2000) Heterogeneity of the local electrostatic environment of the tyrosyl radical in *Mycobacterium tuberculosis* ribonucleotide reductase observed by high-field electron paramagnetic resonance. *J Am Chem Soc* 122(9):1974–1978.
10. Tomter AB, et al. (2011) HF-EPR, Raman, UV/VIS light spectroscopic, and DFT studies of the ribonucleotide reductase R2 tyrosyl radical from Epstein–Barr virus. *PLoS ONE* 6(9):e25022.
11. Un S, Tang XS, Diner BA (1996) 245 GHz high-field EPR study of tyrosine-D zero and tyrosine-Z zero in mutants of photosystem II. *Biochemistry* 35(3):679–684.
12. Ivancich A, Jakopitsch C, Auer M, Un S, Obinger C (2003) Protein-based radicals in the catalase-peroxidase of *synechocystis* PCC6803: A multifrequency EPR investigation of wild-type and variants on the environment of the heme active site. *J Am Chem Soc* 125(46):14093–14102.
13. Dorlet P, et al. (2002) High-field EPR study of tyrosyl radicals in prostaglandin H(2) synthase-1. *Biochemistry* 41(19):6107–6114.
14. Yu MA, et al. (2012) Two tyrosyl radicals stabilize high oxidation states in cytochrome C oxidase for efficient energy conservation and proton translocation. *J Am Chem Soc* 134(10):4753–4761.
15. Ivancich A, Jouve HM, Gaillard J (1996) EPR evidence for a tyrosyl radical intermediate in bovine liver catalase. *J Am Chem Soc* 118:12852–12853.
16. Schünemann V, et al. (2004) Tyrosine radical formation in the reaction of wild type and mutant cytochrome P450cam with peroxy acids: A multifrequency EPR study of intermediates on the millisecond time scale. *J Biol Chem* 279(12):10919–10930.
17. Ivancich A, Mazza G, Desbois A (2001) Comparative electron paramagnetic resonance study of radical intermediates in turnip peroxidase isozymes. *Biochemistry* 40(23):6860–6866.
18. Fasanella EL, Gordy W (1969) Electron spin resonance of an irradiated single crystal of L-tyrosine-HC. *Proc Natl Acad Sci USA* 62(2):299–304.